A Study on Arctic Sea Ice Dynamics Using the Continuous Spin Ising Model

Ellen Wang[1 a)]

AFFILIATIONS

[1] Horace Mann School, Bronx, NY, USA

[a)] Author to whom correspondence should be addressed: ellen.ls.wang@gmail.com

Abstract

The Ising model, initially proposed about 100 years ago to explain ferromagnetism and phase transitions, has become a central pillar of statistical physics and a powerful tool for numerous applications in other fields including environmental studies. In this paper, we introduce continuous spin values between -1 and 1 to a two-dimensional Ising model and utilize the generalized Ising lattice to simulate the dynamics of sea ice/water transition for a large area of 1500km x 1500km in the Arctic region. The simulation process follows the Metropolis-Hastings algorithm and incorporates an innovative factor to account for the inertia of spin value changes. Using the sea ice concentration data collected by the National Snow and Ice Data Center, our model simulation shows striking similarity with the observed ice melting and freezing dynamics. Two numerical measures from the simulation, the average ice coverage and the ice extent, match closely with the observations. Moreover, the model's best-fit parameters demonstrate the substantial impact of the external forces, which can be further enriched and linked to the environmental factors in other climate change models.

Keywords: *Ising model, continuous spin, Metropolis-Hastings algorithm, phase transition, Arctic sea ice, climate change*

I. Introduction

~~The~~ Rapid loss of the Arctic sea ice observed over the past four decades, a strong indicator of global warming, poses serious challenges to the earth. ~~has been an alarming phenomenon that points to drastic global warming, a serious challenge that calls for collective actions by the entire humankind.~~ To accurately predict the Arctic sea ice evolution, which helps prepare for the subsequent environmental and economic impact, therefore has become an urgent task for researchers across many disciplines. The fact that the year 2023 has recorded the ~~has witnessed the most sizzling summer on record and the~~ hottest year in history [1] adds even greater severity to such urgency. As an endeavor to fulfill this task, we innovate upon the classical Ising ~~M~~model in statistical physics. Our study delivers excellent match between model simulations and actual observations, which demonstrates the power of classical physics models in climate change research and presents ample possibilities to further enhance the modeling of the Arctic sea ice dynamics.

A. Ising model

The classical Ising ~~M~~model (IM) is the backbone of this study. It was first formalized by physicists Ernst Ising and Wilhelm Lenz to explain the equilibrium and phase transition in magnetic systems. The one-dimensional (1-D) IM was solved by Ising in his 1924 thesis [2] [3] [4], which proves the non-existence of phase transition in the 1-D IM. In 1944, Lars Onsager [5] was able to solve the two-dimensional (2-D) square-lattice IM analytically. Contradictory to the 1-D case, Onsager identified that there exists a critical temperature $T_c = 2.27 \ J/k_B$ when the phase transition happens in a 2-D IM. Later studies of IM in higher dimensions have been closely associated with various developments in advanced 20th-century physics and mathematical theories, including the transfer-matrix method [6] [7], quantum field theory [8], mean-field theory [9], etc.

Over the years, the IM has found wide success beyond physics. Specifically, the Kinetic IM [9] [10] [11], built upon the equilibrium version, has been proposed to analyze biology, environmental science, machine learning [12] [13], social science, and economic and financial systems. These applications are usually implemented as a discrete time Markov chain of the spin lattice, with spin interactions bounded to finite distance. In biology and neuroscience, IM applications include but are not limited to the condensation of DNA [14], genetics [15], neural networks [16] [17], neuron spike [18], neuron activity in cell assemblies [19], and ligands to receptors binding in cells [20]. In environmental science, the IM has been employed to investigate land pattern dynamics [21] [22]. Recently, Ma, Sudakov, Strong and Golden have successfully used the 2-D IM to capture the essential mechanism of the ice melt ponds equilibrium configuration [23]. In social science, economics, and finance, the IM has been applied to research in urban segregation [24], crisis study [25], stability of money [26], etc.

B. *Arctic sea ice*

The reversible phase transition between water and ice makes the IM a great tool to study the dynamics of a surface region with the co-existence of both states. In this paper, we apply a 2-D IM lattice to study the dynamics of Arctic sea ice melting and freezing cycles, a major climate change indicator that is of significant environmental, economic, and social significance [27].

Sea ice is undoubtedly an integral part of the Arctic Ocean and the earth [27]. In the dark winter months, ice covers almost the entirety of the Arctic Ocean, and the ice extent—defined as the percentage of the areas that are covered by at least 15% ice—and the ice thickness typically reaches its peak around March. Starting in late spring, ice melting gradually exceeds water freezing due to higher temperatures and longer hours of sunlight exposure. Sea ice typically reaches the minimum extent and thickness in mid-September, when ice coverage can drop to under half of the winter maximum [28]. After mid-September, sea water freezing starts to exceed ice melting, so ice coverage expands. This cycle repeats annually.

Ice coverage is widely acknowledged as a crucial indicator of global climate change. Albedo, the percentage of incident light reflected from the surface of the earth, is highly dependent on the ice extent [29]. Light-colored ice or snow reflects more light than blue-colored liquid water; therefore, ice is essential to keeping the Arctic at a cooler temperature and subsequently maintaining the energy balance around the globe. If the energy balance is broken, as ice decline has been detected in recent years, the feedback loop effect may occur, i.e., less reflection and more absorption of solar energy, leading to even more ice loss and further global warming. This is called the ice-albedo feedback effect. Moreover, the Arctic ecosystem is directly impacted by the change in sea ice coverage, which, for instance, threatens the lives of polar bears and walruses who rely on sea ice for hunting and breeding [30].

Data recorded by the National Aeronautics and Space Administration (NASA) and the National Snow and Ice Data Center (NSIDC) since 1979 has shown substantial declines in both ice extent and thickness in the Arctic, despite the year-over-year fluctuations in either direction. The lowest Arctic sea ice extent was observed in September of 2012 [31] [32]; between 2013 and 2022, the ice extent has been higher than the 2012 minimum, but still much lower than the average of the past four decades. July 2023 was reported as the hottest month of the earth on record [33], and 2023 the hottest year on record by a significant margin [1] [34]. Some questions then come to us naturally: how does the Arctic sea ice extent in 2023 compare to the 2012 level? And can our model simulations closely match the comparison observed in the real data? These questions will be addressed in Section V.D.

C. *Outline of the paper*

The goal of this research is to simulate Arctic sea ice dynamics at a large scale using the IM. We will enhance the continuous spin IM [35] [36] to incorporate an innovative factor to account for the inertia to resist spin value changes. The evolution of sea ice/water phase transition will follow the Metropolis-Hastings [37] Monte Carlo process governed by this generalized IM. Based on the Arctic sea ice images collected by the National Snow and Ice Data Center [38] as inputs, our model will output the best-fit Ising parameters and simulated sea ice configurations. The analysis of the numeric measures from these simulation results will validate the applicability of the IM in sea ice studies. In this paper, Section II introduces the theoretical foundation of Ising model; Section III describes the Arctic sea ice data; Section IV illustrates the computational setup; Section V presents the results and analysis, followed by final discussions in Section VI.

II. Theoretical framework

A. Classical Ising model

The system described by an IM is a set of lattice sites, each having a spin that interacts with its neighbors. The Hamiltonian function [2] [3] [4] for the lattice σ in a standard IM is given as

$$H(\sigma) = -\sum_{<i,j>} J_{ij}\sigma_i\sigma_j - \sum_i B_i\sigma_i, \tag{1}$$

where σ_i represents the spin variables at site i, taking the values of $+1$ or -1, J_{ij} represents the interaction between sites, and B_i represents the interaction of the external field with the spin at site i. i and j range across the full lattice, which can be one, two or higher dimensions, and $<i,j>$ represents pairs of spins that interact with each other. In the usual scenario, each spin only interacts with its nearest neighbors, so $<i,j>$ sums over all adjacent sites. For example, in a simple 2-D IM, each spin interacts only with four sites that are directly left, right, above, and below. J_{ij} can be is usually positive values for ferromagnetic and paramagnetic materials,, meaning that adjacent spins are inclined to maintain the same value to achieve low energy or negative values for antiferromagnetic materials.

In statistical physics, the configuration probability follows the Boltzmann distribution [39]:

$$P_\beta(\sigma) = \frac{e^{-\beta H(\sigma)}}{Z_\beta}, \tag{2}$$

where Z_β is the partition function:

$$Z_\beta = \sum_\sigma e^{-\beta H(\sigma)}, \tag{3}$$

and

$$\beta = (k_B T)^{-1}. \tag{4}$$

β is the inverse temperature; k_B is the Boltzmann constant; T is the IM temperature (it is called IM temperature in this paper to differentiate from the ambient temperature that will also be discussed for our sea ice freezing and melting studies).

The evolution of the kinetic IM runs through a series of spin flips over the lattice. The probability of each spin flip depends on whether such a flip increases or reduces the Hamiltonian of the systemenergy. Mathematically the probability is determined by $\min(1, e^{-\beta(H_v - H_\mu)})$ [40], where H_v and H_μ represent the Hamiltonian of the system before and after the flip. It can be easily seen that a higher IM temperature leads to more thermal fluctuations and greater variancesrandomness in the spin value distribution, while a lower IM temperature shows fewerless fluctuations.

B. Continuous sSpin Ising model

Most of the literature studies onof the IM cited in earlier sections [3] [4] [15] [22] [23] focus on binary values of the spins, i.e., σ_i taking values of $+1$ or -1 only. However, the sea ice data for each lattice location takes varying values between 0 and 1 that represent the percentage of ice coverage. Therefore,

4

we generalize the IM to allow for continuous spin values that can take any real number between -1 and $+1$. This generalization enables the IM to examine more realistic systems, but also adds a high degree of complexity to the mathematical solutions. Past research has studied phase transitions and critical behaviors of the continuous IM [35] [36]. Recently, an IM with variable power-law spin strengths was studied with its rich phase diagram [41].

The Hamiltonian function of the continuous spin IM is represented by the same Equation (1). However, σ_i now takes continuous values between $+1$ and -1; $-J_{ij}\sigma_i\sigma_j$ reaches the minimum energy state if $\sigma_i = \sigma_j = +1$, or $\sigma_i = \sigma_j = -1$, as the energy of any other values of the pairs will be higher. The highest energy is observed when $\sigma_i = +1$, $\sigma_j = -1$, or vice versa. This numeric feature works ideally for an ice/water lattice: the most stable low energy state is either 100% water or ice, whereas ice next to water is the most unstable high energy state.

C. Monte Carlo simulation and inertia factor

The incorporation of the continuous spins also adds to the complexity of the Monte Carlo (MC) simulation of the IM lattice. In the classical binary spin IM, σ_i can only flip to $-\sigma_i$ in each simulation step, and therefore the absolute value of the change is always 2 no matter if the flip goes from -1 to $+1$ or from $+1$ to -1. In a continuous IM, the challenge of determining the post-flip numeric value of the new spin arises. In our approach, this new spin is implemented through a random number. However, what is the random distribution that the new spin value should follow? How does the spin value change, i.e. $\Delta\sigma_i$, affect the dynamics of the IM? To address these questions, we introduce an innovative inertia factor I, and the probability of each flip will be determined by

$$P_{flip} = \min\left(1, e^{-\beta(H_v - H_\mu + I|\sigma'_i - \sigma_i|)}\right), \tag{5}$$

Where σ_i represents the original spin value before the change; σ'_i represents the value of the attempted spin change; H_v and H_μ still represent the system Hamiltonian before and after the flip, same as the description for Eq (1) in Section II.A. The newly added $-I|\sigma'_i - \sigma_i|$ accounts for the energy needed to overcome the inertia of the spin change, and I is an IM parameter to be fitted. Intuitively speaking, this term represents the natural resistance to state change, or can be thought of as an analog to the latent heat needed for the ice/water phase transition in classical thermodynamics. Like the total energy change for water/ice phase transition at constant temperature and pressure is proportional to the mass, we choose a linear functional form for the inertia term as the simplest and most sensible assumption. The total energy required for a spin flip is $\Delta E = H_v - H_\mu + I|\sigma'_i - \sigma_i|$, which consists of two parts: the system Hamiltonian change plus the inertia term. The probability of spin value change follows the Boltzmann distribution as Equation (5).

Here is an example to illustrate the inertia effect. Starting with an initial spin value of 0.8, a flip to either 0.7 or 0.6 may result in the same system Hamiltonian value for the new lattice. However, we differentiate these two new states by assigning higher probability for the flip to 0.7 because the spin change is smaller. In Equation (5), $-I|\sigma'_i - \sigma_i|$ determines the distribution of new spin values, and in practice, it significantly improves the simulation results to match the observations.

In summary, the novelty of our IM ~~is twofold~~: we introduce an inertia factor to the classical IM ~~with the~~ continuous spin values ~~and an inertia factor~~ to the study of the critical climate change problem.

These mathematical additions prepare us to study real-world Arctic sea ice dynamics while keeping the computational complexity tractable.

III.   Data description

Our study uses data from the "Near-Real-Time DMSP SSMIS Daily Polar Gridded Sea Ice Concentrations" (NRTSI) dataset [38] collected by the National Snow and Ice Data Center (NSIDC). It captures daily sea ice concentrations for both the Northen and Southern Hemispheres. The Special Sensor Microwave Imager/Sounder (SSMIS) on the NANA Defense Meteorological Satellite Program (DMSP) satellites acquires the near-real-time passive microwave brightness temperatures, which serve as inputs to the NRTSI dataset using the NASA Team algorithm to generate the sea ice concentrations.

The NRTSI files are in netCDF format. Each file of the Arctic region contains a lattice of 448 rows by 304 columns, covering a large earth surface area with the north pole at the center. Each grid cell represents an area of approximately 25 kilometers by 25 kilometers. The value for each grid cell is an integer from 0 to 250 that indicates the fractional ice coverage scaled by 250. 0 indicates 0% ice concentration; 250 indicates 100% ice concentration. The image of part of the NRTSI file on Sept 16th, 2022 is illustrated in Figure 1Figure 1(a). In the map, white represents ice, blue represents water, and

Formatted: Font: 12 pt

6

gray represents land. The exact north pole location is covered by a gray circular mask because of the limitation of the satellite sensor measurement caused by the orbit inclination and instrument swath.
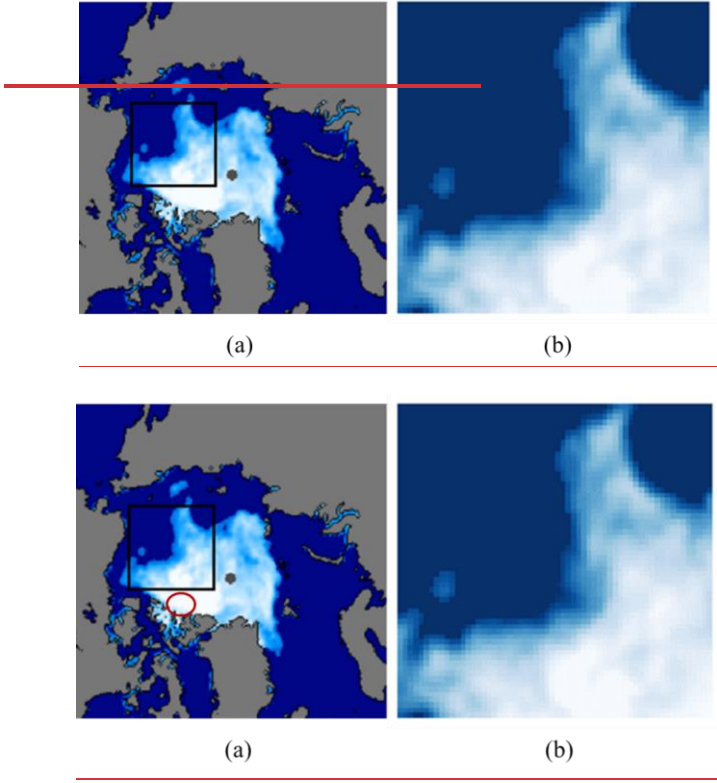
Figure 1: (a) Part of the NRTSI data on Sept 16th, 2022; (b) The focus area for our research, a 60x60 square lattice covering approximately 2.25 million square kilometers.

For this research paper, we focus on studying a specific geographic region bounded by the black square in Figure 1Figure 1(a), ranging from the East Siberian Sea (to the top of the box) and the Beaufort Sea (to the left of the box) to near the polar point; a zoom-in image of this focus area is shown in Figure 1Figure 1(b) . This large square area is unobstructed by land or the north pole mask, making it an ideal field for the IM lattice setup. The area contains 60 rows and 60 columns in the data file, covering approximately 1500km x 1500km, or about 2.25 million square kilometers.

IV.   Ising model lattice and simulation setup

IV.   The purpose of this research is to study the dynamic of ice/water transition for the focus Arctic region. The methodology is outlined as follows. Firstly, we normalize the NRSTI data to a

7

continuous Ising lattice, carefully choose simulation periods, and define the Ising parameters (J, B, I). Secondly, starting from the initial lattice of each simulation period, we run the Metropolis MC simulation based on the set of parameters (J, B, I) to generate a final state of Ising lattice for this period. This full metropolis simulation step is then passed into a numeric optimizer to find the best-fit Ising parameters so that the final Ising lattice matches the observed NRSTI data as closely as possible.

A.   Ising model lattice

We first transform the NRTSI data of the focus region as shown in Figure 1 (b) to Ising-style data. A simple linear mapping is applied to convert integers from 0 to 250 to real numbers from -1 to $+1$. -1 indicates the cell is 100% ice; +1 indicates 100% water; 0 indicates 50%/50% coverage of water/ice. Each cell covers 25km x 25km of the total 1500km x 1500km focus region, and therefore a 60x60 matrix is initialized as the 2-D IM lattice for our study.

B.   Simulation periods

Figure 2Figure 2 (a) and (b) display an example of the initial and the final target states of an IM lattice simulation run. The simulation periods are chosen to be consistently half a month apart, for example, Sept 16th, 2022 in Figure 2Figure 2 (a) and Oct 1st, 2022 in Figure 2Figure 2 (b). This semi-monthly frequency is chosen to balance two considerations. First, the period is sufficiently long to allow for meaningful differentiation of the ice/water configuration between the start and the end dates; second, the period is not excessively too long and allows the IM simulation to mimic the daily ice/water configuration evolution on the interim dates between the start and the end, which is to be illustrated in Section V.B.
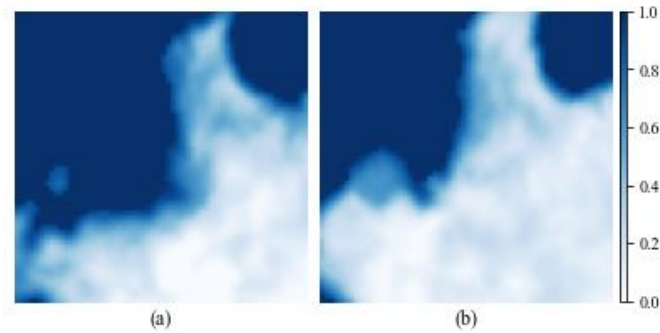
Figure 2: The initial and the final target states of an IM lattice simulation run. (a) shows the actual configuration observed in our focus area on Sept 16th, 2022 and (b) on Oct 1st, 2022. Each full simulation period is half a month. Blue color indicates water; white indicates ice. The darker the color on each cell, the higher the water concentration, as shown by the scale on the right.

C.   Ising model parameters

In the IM Hamiltonian function, i.e., Equation (1), we set the following:

- σ_i is a real number between -1 and $+1$ for any cell i in our focus area.
- $<i,j>$ sums over all adjacent cells, so each spin interacts only with four sites that are directly left, right, above, and below.
- J_{ij} is set to be constant within each simulation period across all cells.
- B_i is set to be time-invariant within each simulation period. However, in order to capture the real-world external force variation across locations, especially the environmental differences from the coast area to the north pole, B_i is set to be a linear function of x_i and y_i coordinates of cell i, i.e. $B_i = B_0 + B_x(x_i - x_0) + B_y(y_i - y_0)$, where B_0 is B at the center of the lattice, and x_0 and y_0 are the coordinates of the lattice center.
- I, the inertia factor, is set to be constant within each simulation period.
- β, the inverse Boltzmann temperature, is set to 1 without loss of generality, because what we are trying to explain is the relative magnitude of (J, B_0, B_x, B_y, I) instead of their absolute values. Similar approach has been taken in other kinetic Ising model research [22].

D. Metropolis simulation steps

Various Monte Carlo (MC) methods have been developed for the IM simulation. Among them the most widely used are the Glauber dynamics [42] and the Metropolis-Hasting algorithm [37]. In our study, we follow the latter for the MC simulation of the IM lattice evolution. As described in Section II.C, an inertia factor is introduced into our model and the generalized Metropolis-Hastings MC steps are below:

1. Select cell i at random from the 2-D lattice of the focus area. Let the spin value of this cell be σ_i.
2. Generate another uniform random variable σ'_i between -1 and $+1$.
3. Compute the energy change ΔH_i from σ_i to σ'_i.
4. Compute the energy $I|\sigma'_i - \sigma_i|$ to overcome the inertia of changing the spin value at i.
5. Compute the total energy change $\Delta E = \Delta H_i + I|\sigma'_i - \sigma_i|$.
6. (a) If ΔE is negative, the energy change is favorable since the energy is reduced. The spin value change is therefore accepted to σ'_i.
   (b) If ΔE is positive, the probability of the spin flip is determined by the Boltzmann distribution. In this case, another uniform random variable r between 0 and 1 is generated. If r is less than $P = e^{-\beta \Delta E}$, the spin value change is accepted; otherwise, the change is rejected and the spin value at i stays at σ_i.

For each semi-monthly simulation period, we repeat the above MC steps 50,000 times. As the lattice of our focus area has 3,600 cells, this repetition allows approximately 14 flip tries for each cell, or roughly once per day. This specific repetition number is chosen by an intuitive pick, which takinges into account the computational complexity of the algorithm and also making sure each spin cell of the Ising lattice gets sufficient attempts to be changed. Obviously, other Other choices of the repetition number can be considered as well. The fitted parameter values (J, B_0, B_x, B_y, I) might vary with different repetition numbers. What is important is to ensure the repetition number for each period is proportional to its duration, so the unit time of each metropolis step is the same across the full simulation process [22].

9

E. Dual annealing optimization

If we follow the Metropolis MCMC simulation starting from an initial state of certain sea ice configuration as described in the above section, the Ising parameters (J, B_0, B_x, B_y, I) will dictate the sea ice evolution process. Different parameter regimes shall lead to varying final states. For this application on sea ice, the spin interaction coefficient J should be positive, because adjacent cells will exert positive influence on each other, thereby maintaining similar values. Similarly, the inertia factor I is also expected to be positive, due to the resistance to state change in the ice/water phase transition. The external force parameters, $B_0, B_x,$ and B_y shall display wider variances, which could be explained by the seasonal and geographical environmental effects.

Our goal is to match the observed final state lattice configuration as closely as possible upon the completion of the IM simulations. In this research, the similarity between the observed and the simulated lattice configurations is measured by the sum of the absolute spin value differentials across the lattice. Mathematically, this is the Manhattan distance (as opposed to the more commonly used Euclidean distance) between the observed and the simulated matrices.

Finally, we fit the values of parameters (J, B_0, B_x, B_y, I) to maximize of the similarity measure, i.e., to minimize the sum of the absolute spin value differentials. The minimization is done with the dual annealing optimization method, which combines fast local search with classical simulated annealing to achieve the global minimization solution [43] [44]. Description of the dual annealing method can be found in the Python SciPy package.

V. Results

We employ the continuous spin IM to simulate the dynamics of the sea ice/water transition for the focus Arctic Sea area. Thanks to the NRTSI data, we can conduct the simulation for every year in the past four decades.

A. Simulation results for 2022

We start with the results for the year 2022.

Figure 3Figure 3 shows the semi-monthly NSIDC sea ice images of our focus area from June 16th, 2022 to Jan 1st, 2023. As can be seen, the melting cycle starts from June 16th and goes until Sept 16th, and the freezing cycle from Sept 16th to year end. Prior to June 16th, the region is almost fully covered by ice, so the IM simulation will be trivial. This is why we set the simulation start date on June 16th of each year. During the period of June 16th to Dec 16th, every successiveeding image shows considerable ice coverage difference from the previous date while retaining certain core features. This semi-monthly frequency choice allows our IM simulation to capture the essence of the evolution dynamics without overfitting the model.
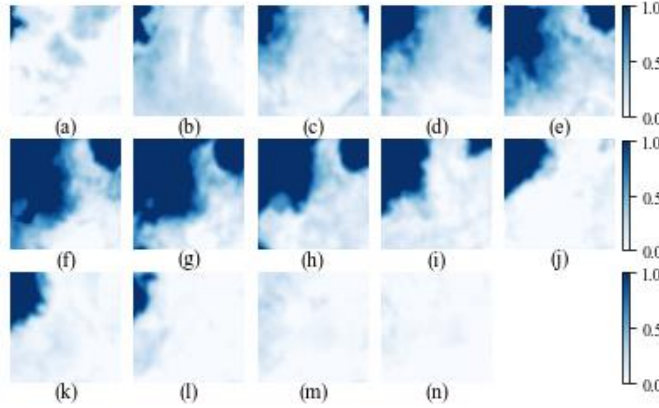
Figure 3: The actual semi-monthly evolution of sea ice in our focus area in 2022: (a) June 16th, (b) July 1st, (c) July 16th, (d) Aug 1st, (e) Aug 16th, (f) Sept 1st, (g) Sept 16th, (h) Oct 1st, (i) Oct 16th, (j) Nov 1st, (k) Nov 16th, (l) Dec 1st, (m) Dec 16th, 2022, and (n) Jan 1st, 2023.

The best-fit Ising parameters (J, B_0, B_x, B_y, I) for each simulation period are shown in Table 1Table 1. The spin interaction coefficient J and the inertia factor I are relatively stable across periods. On the other hand, the external force parameters B_0, B_x, and B_y display large variations across different time periods. This matches our intuition, because J and I represent the inherent interactions in the water/ice system; it is natural that the strength of such interactions does not change much across different time periods. J remaining positive across all periods shows that adjacent cells are inclined to maintain values of the same sign, i.e., the area surrounding ice will be more likely to freeze, and area surrounding water will tend to melt, which matches our intuition too. In this sense, the ice/water system displays the feature of ferromagnetism/paramagnetism instead of antiferromagnetism. On the other hand, the external force parameters B_0, B_x, and B_y display large variations across different time periods. In particular, the average force B_0 is positive from June 1st to Sept 16th but turns negative afterwards, which can be explained intuitively by the seasonal ambient temperature as the dominant external factor for ice/water dynamics. Ambient temperature is not the only factor, though. Arctic temperature usually peaks in July/August while B_0 remains positive and ice melting continues through mid-September. This lagging effect could be explained by other environmental effects such as albedo or jet streams but is beyond the scope of this study. The values of B_x and B_y are negative overall, which can be understood geographically. For our focus area as illustrated in Figure 1, x coordinate corresponds to the rows of the lattice, going incrementally from top to bottom; y coordinate corresponds to the columns of the lattice going incrementally from left to right. Interestingly, ice coverage at the bottom area, the Canadian Arctic Archipelago, is much thicker than elsewhere including the north pole (the gray circular mask). In fact, many scientists believe this region will be the last piece of ice standing in the Arctic if the Blue Ocean Event happens [45]. Because the lower part of the focus area is usually covered by more ice, it explains why B_x is usually negative, except for very few periods when the ice coverage remains relatively unchanged. Similarly, higher y coordinate goes in the direction toward the north pole, therefore usually colder and covered by more ice. The values of B_x and B_y show more fluctuations than other parameters, indicating that our simplified linear functional form of $B_i = B_0 + B_x(x_i - x_0) + B_y(y_i - y_0)$ is far

11

from perfectly modeling the full effect of external field; it can be further enriched by linking to actual geographical and environmental factors to enhance the power of the Ising model in the future, which is out of scope of this paper.

	6/16 to 7/1	7/1 to 7/16	7/16 to 8/1	8/1 to 8/16	8/16 to 9/1	9/1 to 9/16	9/16 to 10/1	10/1 to 10/16	10/16 to 11/1	11/1 to 11/16	11/16 to 12/1	12/1 to 12/16	12/16 to 1/1/2023
J	2.3	2.6	2.3	2.4	2.7	2.3	2.6	2.7	2.6	2.5	2.3	2.7	2.7
B_0	7.0	2.0	6.5	9.1	4.3	3.6	-12.6	-12.7	-14.9	-9.6	-15.0	-13.1	-14.4
B_x	0.2	-9.7	-5.5	3.7	-7.5	-8.2	-10.0	-6.1	-8.5	9.7	-1.9	-0.8	-3.1
B_y	-10.0	3.0	3.7	1.0	-6.4	2.9	0.1	-8.4	-5.6	-10.0	-5.9	5.4	-8.0
I	10.3	9.1	11.0	10.8	10.7	10.9	10.6	9.3	9.4	10.4	9.1	10.9	10.8

Table 1: The best-fit Ising parameters for the 2022 sea ice evolution.

The simulated sea ice images for each 2022 period are shown in Figure 4 utilizing the best-fit Ising parameters in Table 1. These images exhibit excellent similarity to Figure 3, demonstrating the strong explanatory power of our Ising model. Nevertheless, our model is far from being perfect. Upon close inspection, The images in Figure 3 and Figure 4 do reveal discrepancies, especially as shown in image (d) and (e) for Aug 1st and 16th, 2022 respectively, where the actual ice configurations display significant irregularity compared to the prior period. While an IM with simple parameterization encounters difficulties in describing these local irregularities, it is feasible to include a richer set of parameters or to employ more complicated parametric functional forms at the potential cost of overfitting. In this paper, we keep our Ising model tractable and accept these local discrepancies.
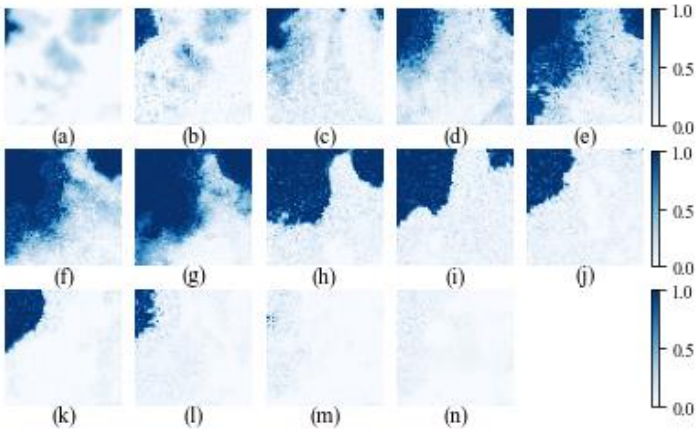
Figure 4: The simulated semi-monthly evolution of sea ice for our focus area in 2022. (a) is the actual image on June 16th, 2022 as the start state; (b) - (n) are simulated images on (b) July 1st, (c) July 16th, (d) Aug 1st, (e) Aug 16th, (f) Sept 1st, (g) Sept 16th, (h) Oct 1st, (i) Oct 16th, (j) Nov 1st, (k) Nov 16th, (l) Dec 1st, (m) Dec 16th, and (n) Jan 1st, 2023.

To quantify the similarity between the IM simulations and the observations, the absolute differences of the ice percentage between each of the images in Figure 3 and Figure 4 are calculated; the results are

shown as the heatmaps in Figure 5 (a) – (n). The error bar plot in Figure 5 (O) shows the overall average differential for the whole focus area for each period. In these heatmaps, light yellow color indicates that the actual and simulated images match well, whereas locations with higher discrepancy are colored as red. The heatmaps are very revealing: the small red patches mostly appear around the boundaries between water and ice, which shows that the majority of the discrepancy between the simulated and actual images happens around these border areas. This is not surprising: the IM cannot perfectly model these boundary granularities, but it does a good job at capturing the overall configuration.
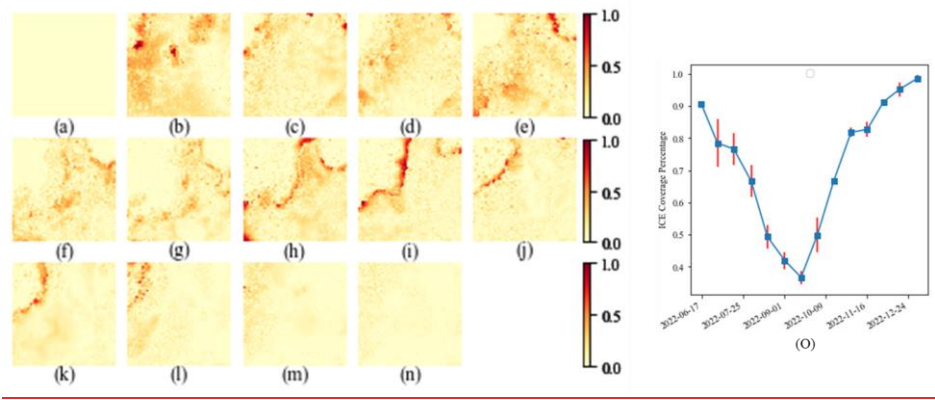
Figure 5: (a) - (n) Heatmaps illustrating the absolute difference of the ice percentage between Figure 3 and 4 for each semi-monthly period, from (a) Jun. 16th, 2022 to (n) Jan. 1st, 2023. (O) Error bar plot showing the average ice percentage differential over these periods.

Wewe also compute two key numerical measures for our focus area: the average ice coverage percentage, i.e., the mean of the ice coverage percentage over the lattice, and the ice extent, i.e., the percentage of areas that are covered by at least 15% ice. The comparison results are shown in Figure 6Figure 5. As anticipated, we see an excellent match in both figures as a result of the superior explanatory power of our IM, although the results do show marginal but non-trivial discrepancy, consistent with what is shown in Figure 5. It is interesting to note that the simulated average ice coverage is usually slightly higher than the actual measures, but the simulated ice extent is slightly lower than the actual, a pattern that can be further investigated in future research.
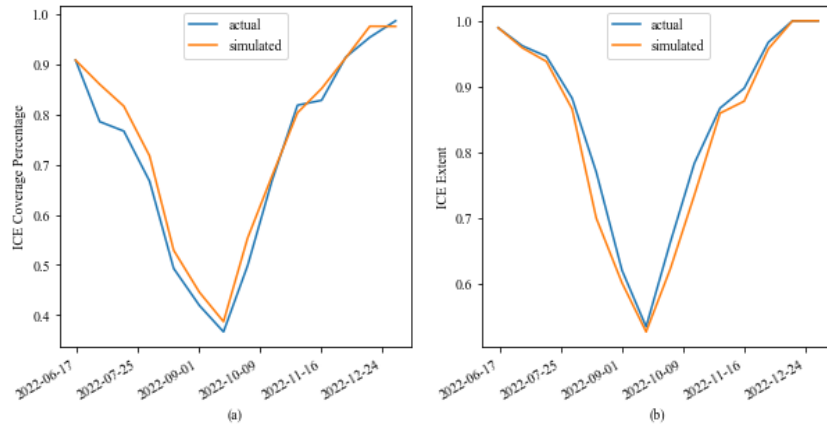
Figure 6: (a) The average ice coverage percentage in our focus area from June 16th, 2022 to Jan 1st, 2023; (b) The sea ice extent (the percentage of areas with at least 15% ice coverage) for the same period. Blue curves are the actual measures from the NRTSI data; orange ones show the IM simulation results.

B. Daily sea ice evolution in 2022

Do our semi-monthly IM simulation results match the actual sea ice dynamics on a smaller time scale? To answer this question, we utilize the semi-monthly Ising parameters in Table 1Table 1 to simulate the daily evolution in 2022. Two periods, a melting period from Aug 16th to Sept 1st, 2022, and a freezing period from Oct 16th to Nov 1st, 2022, are simulated day-by-day for this experiment. The results, with comparisons between the actual and the simulated daily ice evolution, are shown in Figure 7Figure 6, Figure 8Figure 7, Figure 9Figure 8, and Figure 10Figure 9 respectively. The comparisons exhibit striking similarity across all the daily images in both periods, confirming that our IM preserves the the more granular ice/water dynamics in shorter time scale.
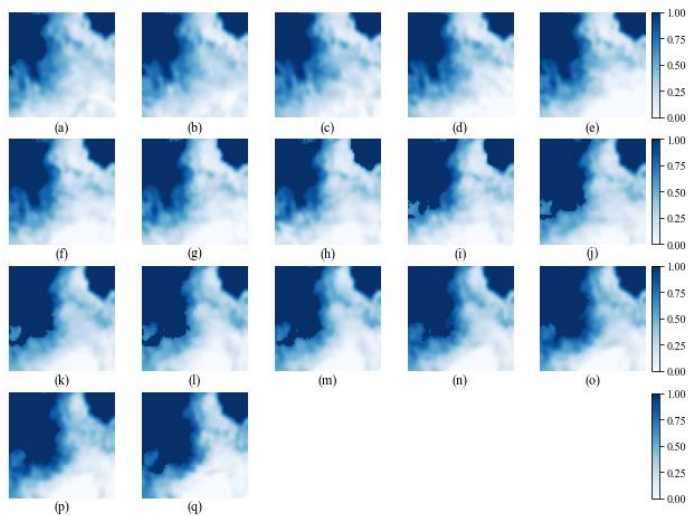
Figure 76: The actual daily evolution of sea ice in our focus area during a melting cycle from (a) Aug 16th to (q) Sept 1st, 2022.
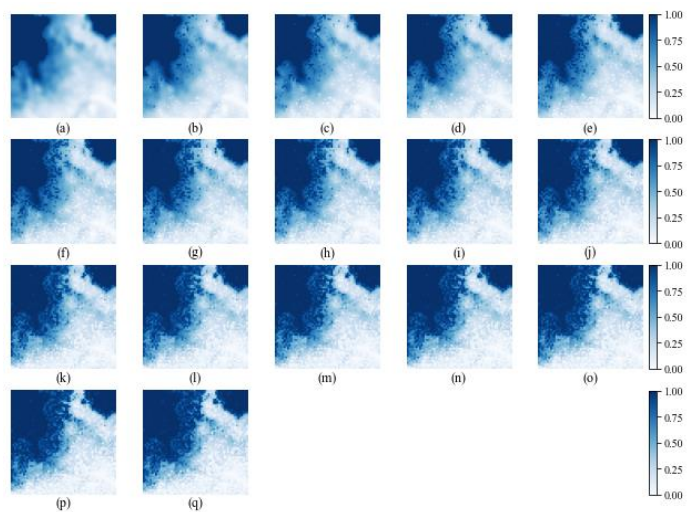
Figure 87: The simulated daily evolution of sea ice, based on the semi-monthly Ising parameters, for our focus area during a melting cycle from (a) Aug 16th to (q) Sept 1st, 2022.
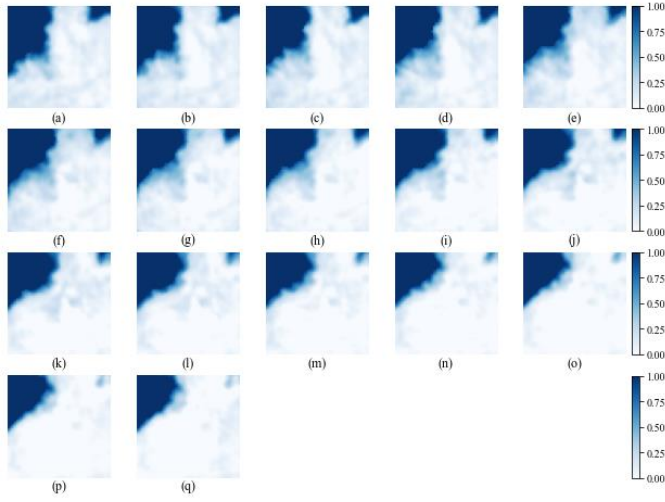
Figure 98: The actual daily evolution of sea ice in our focus area during a freezing cycle from (a) Oct 16th to (q) Nov 1st, 2022.
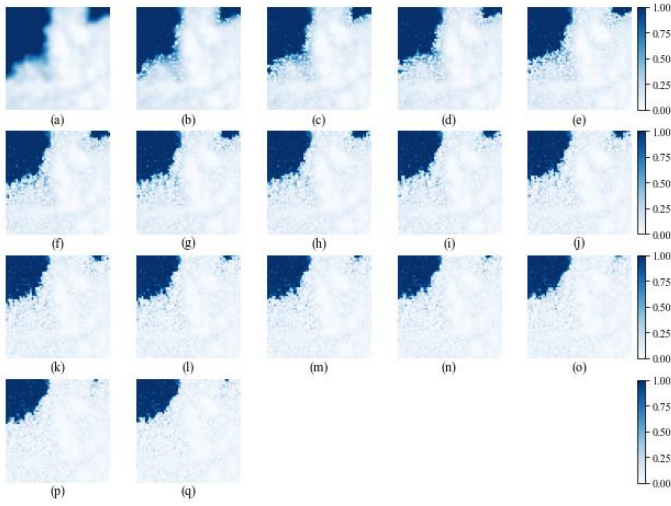

Figure 109: The simulated daily evolution of sea ice, based on the semi-month Ising parameters, for our focus area during a freezing cycle from (a) Oct 16th to (q) Nov 1st, 2022.

C.   Simulation results for 2023

2023 has recorded is on track to be the hottest year on record [1] [34] and is therefore a critical year for our study. Figure 11Figure 10 shows the observed semi-monthly sea ice evolution from June 16th to Dec 1st in 2023 for our focus area. New data can certainly be included in this study in the future once it is collected. It can be observed that water covered approximately 75% of the area in peak September this year.
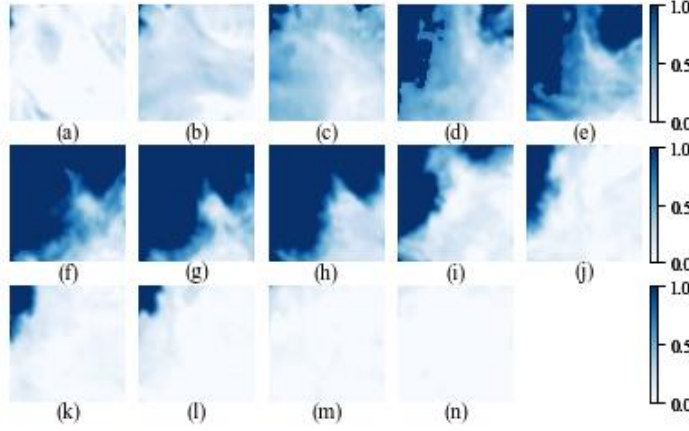

Figure 1110: The actual semi-monthly evolution of sea ice in our focus area in 2023: (a) June 16th, (b) July 1st, (c) July 16th, (d) Aug 1st, (e) Aug 16th, (f) Sept 1st, (g) Sept 16th, (h) Oct 1st, (i) Oct 16th, (j) Nov 1st, (k) Nov 16th, (l) Dec 1st, (m) Dec 16th, and (n) Jan 1st, 2024

Following the same steps as in Section V.A, IM simulations are conducted for 2023 for the focus area. The best-fit Ising parameters are listed in Table 2Table 2, the simulated images shown in Figure 12Figure 11, and the comparisons for the average ice coverage percentage and the ice extent illustrated in Figure 13Figure 12. Like the 2022 results in Section V.A, excellent match is observed between the IM simulation and the actual sea ice evolution. As can be seen, the simulated sea ice extent drops to nearly 30% in Sept 2023 for our focus area, much lower than the September 2022 level in Figure 6Figure 5.

	6/16 to 7/1	7/1 to 7/16	7/16 to 8/1	8/1 to 8/16	8/16 to 9/1	9/1 to 9/16	9/16 to 10/1	10/1 to 10/16	10/16 to 11/1	11/1 to 11/16	11/16 to 12/1	12/1 to 12/16	12/16 to 1/1/2024
J	2.3	2.3	2.4	2.3	2.3	2.6	2.3	2.7	2.5	2.7	2.4	2.7	2.7
B_0	7.5	7.2	5.2	6.0	7.5	2.6	-1.0	-14.9	-14.7	-12.9	-13.8	-14.7	-15.0
B_x	-0.4	-2.0	-6.7	-7.3	-9.3	-7.3	2.5	-9.5	-4.7	-9.6	-9.3	9.3	-0.3
B_y	-2.0	-3.9	-8.0	5.2	-6.1	-1.8	-9.8	-7.9	-6.3	4.0	-2.4	-3.2	-4.8
I	10.0	10.9	10.8	11.0	10.8	11.0	11.0	10.0	9.5	10.5	9.5	10.5	10.9

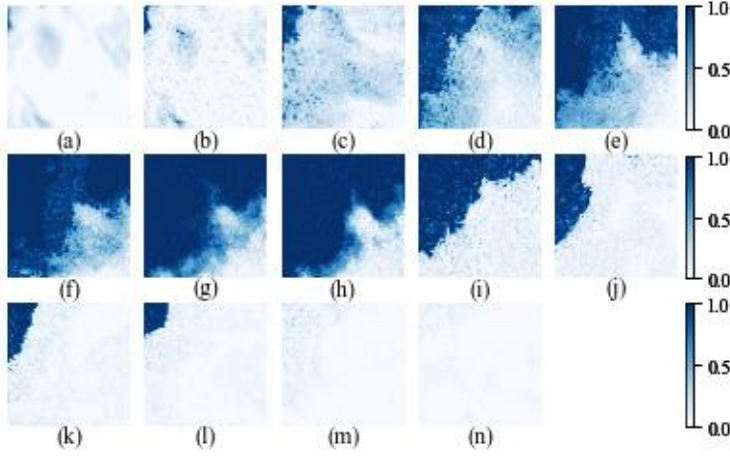Table 2: The best-fit Ising parameters for the 2023 sea ice evolution.

Figure 12~~11~~: The simulated semi-monthly evolution of sea ice in our focus area arctic sea in 2023. (a) is the actual image on June 16th as the start state; (b) - (l) are simulated images on (b) July 1st, (c) July 16th, (d) Aug 1st, (e) Aug 16th, (f) Sept 1st, (g) Sept 16th, (h) Oct 1st, (i) Oct 16th, (j) Nov 1st, (k) Nov 16th, (l) Dec 1st, (m) Dec 16th, and (n) Jan 1st, 2024
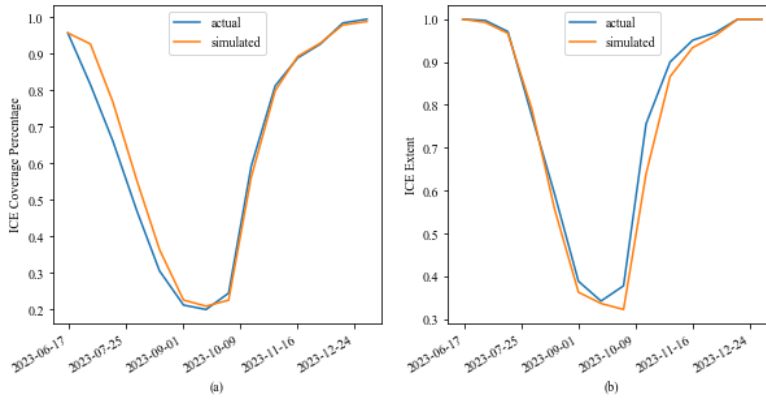

Figure 13~~12~~: (a) The average ice coverage percentage in our focus area from June 16th to Dec 1st, 2023; (b) The sea ice extent (the percentage of areas with at least 15% ice coverage) for the same period. Blue curves are the actual measures from the NRTSI data; orange ones show the IM simulation results.

D. Comparison of sea ice extent between 2023 and 2012

2012 recorded the lowest September Arctic sea ice extent in history [46], while 2023 witnessed the hottest July and is projected to be the hottest year. It would be an interesting experiment to compare the 2023 sea ice extent to that in 2012.

18

Following the same steps as in Section V.A and Section V.C, the IM simulations are conducted for the period of June 16th, 2012 to Jan 1st, 2013 for the focus area. To keep the paper concise, we will skip the semi-monthly actual and simulated images and the best-fit parameters, which can be found in the Supplementary Material. The more informative ice coverage and extent comparison charts are nevertheless included in Figure 14Figure 13.
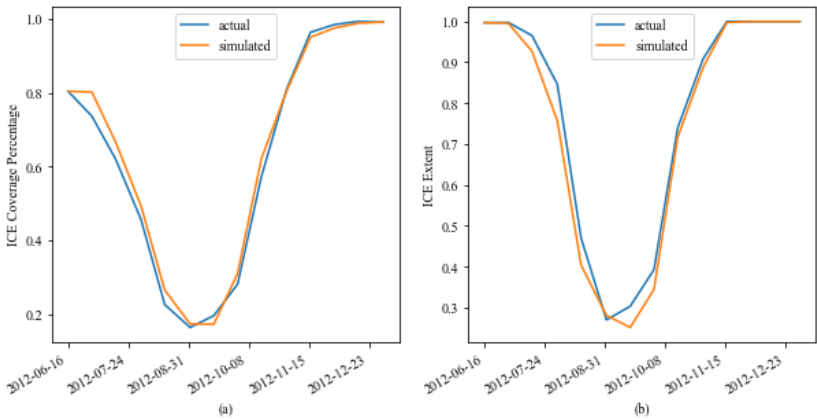

Figure 1413: (a) The average ice coverage percentage in our focus area from June 16th, 2012 to Jan 1st, 2013; (b) The sea ice extent (the percentage of areas with at least 15% ice coverage) for the same period. Blue curves are the actual measures from the NRTSI data; orange ones show the IM simulation results.

Comparing Figure 13Figure 12 with Figure 14Figure 13 indicates that 2023 did not break the record low Arctic sea ice extent level set in 2012, validated by both the actual measures and the IM simulations. However, 2023 sets the second lowest ice extent for our focus area, below those low levels previously achieved in 2019 and 2020[1] (2019 and 2020 results are not included in this paper but can be provided upon request.) Even though 2023 does not break the historical record, it offers no reason for us to be optimistic about the future. In fact, in the 45-year-satellite record from 1979 to 2023, 17 of the lowest minimums have all occurred in the last 17 years [47]. Many scientists are concerned that the effect of Arctic sea ice decline on global warming will intensify as the sea ice loss continues [48] [49]. Although predicting the sea ice extent for the future years is beyond the scope of our current study, we will discuss the possibilities and issues in the next section.

VI.   Discussion and future work

In this paper, we innovatively introduce continuous spin values and an inertia factor to a classical 2-D IM, which is utilized to simulate the dynamics of the sea ice evolution in the Arctic region by employing the Metropolis-Hastings algorithm. Our results show excellent similarity with the actual sea ice dynamics, based on the ice configuration images and the numerical measures including the average

19

---

[1] For the entire Arctic region not limited to our focus area, 2023 marks the 6th-lowest ice extent in history [47]; all 6 minimums are well within small margins.

ice coverage and the ice extent. This demonstrates ~~It is exciting and inspiring to see~~ that the 100-year-old classical Ising model can be applied to significantly contribute ~~has the potential to bring enormous power~~ towards climate change research and other applied science studies.

A. Discussions on the Ising model methodology

How is the extrapolation ability of the model? In other words, how does the model perform if applying the Ising parameters fitted from one year to the data of another year? For this purpose, we tested the projection of Sept. to Dec. 2023 based on Aug. 2023 ice configuration and the 2022 best-fit parameters in Table 1. The extrapolating results show slightly larger variances compare to Figure 12, because The idiosyncratic intra-year configurations will not be fully reproduced by the Ising parameters from a different year. However, the ice percentage and extent metrics have correctly predicted that Sept 2023 would experience the second lowest ice extent in history for our focus Arctic sea ice area. This shows that recycling the Ising parameters, even though far from perfect, can provide us with a lot of insights across different years.

Also interesting is the effect of introducing the inertia factor I. For this, we have explored the vanilla Ising model without the inertia term; the corresponding simulation results significantly underperform the results with the inertia term in Section V. This demonstrates that the inertia term has significant strength toward sea ice modeling, indicating that Arctic sea ice and water have a tendency to stay unchanged. However, this does not mean that the inertia factor is a must-have; it could be possible to improve the Ising model performance via other routes, e.g. further enriching the functional forms of the external force B, which is out of scope of this paper.

Details of the above analyses are not included due to the length constraints of the paper, but will be provided upon reasonable request.

~~A.~~ B. Will a "Blue Ocean Event" happen? If so, when will it be?

Arctic sea ice extent in September 2023 was near the historic minimum achieved in 2012. As the Arctic sea ice continues to shrink, will a "Blue Ocean Event" happen, i.e., will we see an "ice-free" Arctic Ocean? Some research predicts that this can happen in the 2030s [48].

Our current study will need to be extended to gain the full predictive power when utilized to answer this "Blue Ocean Event" question. As shown in Table 1 ~~Table 1~~ and Table 2 ~~Table 2~~, the best-fit IM parameters demonstrate the substantial impact of the external force factor B, which remains unexplored within the scope of our model. If the functional form of this external force is further enriched and linked to actual environmental factors in climate change modeling, the IM framework may prove its strength in offering the "Ising model Prediction" to answer the "Blue Ocean Event" question.

~~B.~~ C. Quantum Ising Model

Our study sets the stage for future Ising model research on sea ice evolution. Methodologically, we generalize the classical Ising model with continuous spin values to incorporate varying ice/water percentages across the Ising lattice. Another possible but more complicated idea to be explored in

future research is the qQuantum Ising mModel (QIM), or the so-called tTransverse fField Ising mModel [50] [51]. With quantum computers, the continuous spin values can be naturally modeled by the rotation of qubits in the Bloch Sphere [52]. Large quantum computers are inaccessible for personal usage currently [53]; but once they are reachable, our research can be readily extended with the assistance of quantum computing in the future.

Author Declarations

Conflict of Interest

The authors have no conflicts to disclose.

Data Availability

The Near-Real-Time DMSP SSMIS Daily Polar Gridded Sea Ice Concentrations" (NRTSI) data used in this study are publicly available on National Snow and Ice Data Center (NSIDC) website https://nsidc.org/data/nsidc-0081/versions/2. The data used in this paper can also be provided from the corresponding author upon reasonable request.

References

[1] NOAA National Centers for Environmental Information, "Climate.gov," Januray 2024. [Online].
Available: https://www.climate.gov/news-features/featured-images/2023-was-warmest-year-
modern-temperature-
record#:~:text=The%20year%202023%20was%20the,decade%20(2014%E2%80%932023).

[2] E. Ising, "Beitrag zur Theorie des Ferromagnetismus," *Z. Phys,* vol. 31, no. 1, p. 2530258, 1925.

[3] E. Ising, Contribution to the Theory of Ferromagnetism, 1924.

[4] S. G. Brush, "History of the Lenz-Ising model," *Review of Modern Physics,* vol. 39, no. 4, p.
883, 1967.

[5] L. Onsager, "Crystal statistics. I. A two-dimensional model with an order-disorder transition,"
Physical Review, vol. 65, no. 3-4, pp. 117-149, 1944.

[6] H. A. Kramers and G. H. Wannier, "Statistics of the Two-Dimensional Ferromagnet. Part I,"
Physical Review, vol. 60, no. 3, pp. 252-262, 1941.

[7] H. A. Kramers and G. H. Wannier, "Statistics of the Two-Dimensional Ferromagnet. Part II,"
Physical Review, vol. 60, no. 3, pp. 263-176, 1941.

[8] J. Zuber and C. Itzykson, "Quantum field theory and the two-dimensional Ising model,"
Physical Review D, vol. 15, p. 2875, 1977.

[9] M. Aguilera, S. A. Moosavi and H. Shimazaki, "A unifying framework for mean-field theories,"
Nature Communications, vol. 12, p. 1197, 2021.

[10] S. Sides, P. Rikvold and M. Novotony, "Kinetic Ising model in an oscilating field: finite-size
scaling at the dynamic phase transition," *Physical review letters,* vol. 81, no. 4, p. 4865, 1998.

[11] D. Stauffer, "Social applications of two-dimensional Ising models," *American Journal of
Physics,* vol. 76, no. 4, pp. 470-473, 2008.

[12] C. Campajola, F. Lillo and D. Tantari, "Inference of the kinetic Ising model with heterogeneous
missing data," *Physical Review E,* vol. 99, no. 6, p. 062138, 2019.

[13] B. Dun and Y. Roudi, "Learning and inference in a nonequilibrium Ising model with hidden nodes," *Physical Review E,* vol. 87, no. 2, p. 022127, 2013.

[14] N. N. Vtyurina, D. Dulin, M. W. Docter, A. S. Meyer, N. H. Dekker and E. A. Abbondanzieri, "Hysteresis in DNA compaction by Dps is described by an Ising model," *Proceedings of the National Academy of Sciences,* vol. 113, no. 18, pp. 4982-4987, 2016.

[15] J. Majewski, H. Li and J. Ott, "The Ising model in physics and statistical genetics," *The American Journal of Human Genetics,* vol. 69, no. 4, pp. 853-862, 2001.

[16] A. Witoelar and Y. Roudi, "Neural network reconstruction using kinetic Ising models with memory," *BMC Neurosci.,* vol. 12, p. 274, 2011.

[17] C. Donner and M. Opper, "Inverse Ising problem in continuous time: a latent variable approach," *Physical Review E,* vol. 96, p. 061104, 2017.

[18] J. Hertz, Y. Roudi and J. Tyrcha, "Ising model for inferring network structure from spike data," *arXiv.1106.1752,* 2011.

[19] Y. Roudi, D. B. and J. Hertz, "Multi-neuronal activity and functional connectivity in cell assemblies," *Curr. Opin. Neurobiol,* vol. 32, p. 38, 2015.

[20] Y. Shi and T. Duke, "Cooperative model of bacteril sensing," *Physical Review E,* vol. 58, no. 5, pp. 6399-6406, 1998.

[21] T. F. Stepinski, "Spatially explicit simulation of deforestation," *Environmental Research: Ecology.*

[22] T. F. Stepinski and J. Nowosad, "The kinetic Ising model encapsulates essential dynamics of land pattern change," *bioRxiv,* 2023.

[23] Y.-P. Ma, I. Sudakov, C. Strong and K. Golden, "Ising model for melt ponds on Arctic sea ice," *New Journal of Physics,* vol. 21, p. 063029, 2019.

[24] T. C. Schelling, "Dynamic models of segregation," *J. Math. Sociol.,* vol. 1, pp. 143-186, 1971.

[25] J. P. Bouchaud, "Crises and collective socio-economic phenomena: simple," *J. Stat. Phys.,* vol. 151, p. 567, 2013.

[26] S. Bornholdt and F. Wagner, "Stability of money: phase transitions," *Physica A: Statistical Mechanics and its Applications,* vol. 316, no. 1-4, pp. 453-468, 2002.

[27] United States Environmental Protection Agency, "Climate Change Indicators: Arctic Sea Ice," 2021. [Online]. Available: https://www.epa.gov/climate-indicators/climate-change-indicators-arctic-sea-ice#:~:text=September%20is%20typically%20when%20the,maximum%20extent%20after%20winter%20freezing..

[28] R. Lindsey and M. Scott, "Climate Change: Arctic sea ice summer minimum," *Climate.gov,* 2022.

[29] NASA Langley Research Center's Atmospheric Science Data Center, "Ice-Albedo Feedback in the Arctic," *NASA,* 2020.

[30] K. L. Oakley, M. E. Whalen, D. C. Douglas, M. S. Udevitz, T. C. Atwood and C. Jay, "USGS - Science for a changing world," 2012. [Online]. Available: https://pubs.usgs.gov/publication/fs20123131.

[31] NSIDC, "Arctic sea ice news and analysis," 2021.

[32] NSIDC, "EASE-Grid sea ice age, version 4," 2021.

[33] World Meteorological Organization, "Copernicus confirms July 2023 was the hottest month ever recorded," 2023.

[34] Copernius, "Record warm November consolidates 2023 as the warmest year," 2023. [Online]. Available: https://climate.copernicus.eu/record-warm-november-consolidates-2023-warmest-year#:~:text=The%20extraordinary%20global%20November%20temperatures,Climate%20Change%20Service%20(C3S).

[35] G. S. Sylvester and H. van Beijeren, "Phase Transitions for Continous-Spin Ising Ferromagnets," *Journal of Functional Analysis,* vol. 28, pp. 145-167, 1978.

[36] E. Bayong and H. T. Diep, "Effect of long-range interactions on the critical behavior of the continuous Ising model," *Physical Review B,* vol. 59, no. 18, p. 11919, 1999.

[37] N. Metropolis, A. W. Rosenbluth, M. N. Rosenbluth, A. H. Teller and E. Teller, "Equation of State Calculations by Fast Computing Machines," *J. Chem Phys,* vol. 21, no. 6, p. 1087, 1953.

24

[38] W. Meiser, J. Steward, H. Wilcox, M. Hardman and D. Scott, "Near-Real-Time DMSP SSMIS Daily Polar Gridded Sea Ice Concentrations, Version 2," NASA National Snow and Ice Data Center Distributed Active Archive Center, Boulder, Colorado USA, 2023.

[39] L. Boltzmann, "Studies on the balance of living force between moving material points," *Wiener Berichte,* vol. 58, pp. 517-560, 1868.

[40] A. Shekaari and M. Jafari, "Theory and simulation of the Ising model," *arXiv,* 2021.

[41] M. Krasnytska, B. Berche, Y. Holovatch and R. Kenna, "Ising model with variable spin/agent strengths," *Journal of Physics: Complexity,* vol. 1, p. 035008, 2020.

[42] G. J. Roy, "Time-Dependent Statistics of the Ising Model," *Journal of Mathematical Physics,* vol. 4, no. 2, pp. 294-307, 1963.

[43] C. Tsallis and D. Stariolo, "Generalized Simulated Annealing," *Physica A,* vol. 233, pp. 395-406, 1996.

[44] Y. Xiang, D. Sun, W. Fan and X. Gong, "Generalized Simulated Annealing Algorithm and Its Application to the Thomson Model," *Physics Letters A,* vol. 233, pp. 216-220, 1997.

[45] Y. Hu, R. M. Horton, M. Song and J. Liu, "Reducing spread in climate model projections of a September ice-free Arctic," *Proceedings of the National Academy of Sciences,* vol. 110, no. 31, p. 12571–12576, 2013.

[46] NASA , "Arctic Sea Ice Minimum Extent," 2022.

[47] "Arctic sea ice minimum at sixth lowest extent on record," National Snow & Ice Data Center,, 2023. [Online]. Available: https://nsidc.org/arcticseaicenews/2023/09/arctic-sea-ice-minimum-at-sixth/.

[48] Y.-H. Kim, S.-K. Min, N. P. Gillett, D. Notz and E. Malinina, "Observationally-constrained projections of an ice-free Arctic even under a low emission scenario," *Nature Communications,* vol. 14, p. 3139, 2023.

[49] G. Peng, J. L. Matthews, M. Wang, R. Vose and L. Sun, "What Do Global Climate Models Tell Us about Future Arctic Sea Ice Coverage Changes?," *Climate,* vol. 8, no. 15, p. 1, 2020.

[50] P. Pferty, "The one-dimensional Ising model with a transverse field," *Annals of Physics,* pp. 79-90, 1970.

[51] B. K. Chakrabarti, A. Dutta and P. Sen, Quantum Ising Phases and Transitions in Transverse Ising Models, Berlin: Springer, 1996.

[52] M. A. Nielsen and I. L. Chuang, Quantum Computation and Quantum Information, Cambridge University Press, 2004.

[53] M. I. Dyakonov, Will We Ever Have a Quantum Computer?, Springer, 2020.